Chemical Science

H₂

H₂

CuCrO₂

ROYAL SOCIETY
OF CHEMISTRY

EDGE ARTICLE
Erwin Reisner *et al.*
Solar H₂ generation in water with a CuCrO₂ photocathode modified
with an organic dye and molecular Ni catalyst

EDGE ARTICLE

Check for updates

Solar H_2 generation in water with a $CuCrO_2$ photocathode modified with an organic dye and molecular Ni catalyst†

Charles E. Creissen, Julien Warnan and Erwin Reisner [ID] *

Dye-sensitised photoelectrochemical (DSPEC) cells have emerged in recent years as a route to solar fuel production. However, fuel-forming photocathodes are presently limited by photo-corrodible narrow band gap semiconductors or the small range of available wide bandgap p-type semiconductors such as NiO that display low performance with dyes. Here, we introduce $CuCrO_2$ as a suitable p-type semiconductor for visible light-driven H_2 generation upon co-immobilisation of a phosphonated diketopyrrolopyrrole dye with a Ni-bis(diphosphine) catalyst. The hybrid $CuCrO_2$ photocathode displays an early photocurrent onset potential of +0.75 V *vs.* RHE and delivers a photocurrent of 15 μA cm^{-2} at 0.0 V *vs.* RHE in pH 3 aqueous electrolyte solution under UV-filtered simulated solar irradiation. Controlled potential photoelectrolysis at 0.0 V *vs.* RHE shows good stability and yields a Ni catalyst-based turnover number of 126 ± 13 towards H_2 after 2 h. This precious metal-free system outperforms an analogous NiO|dye/catalyst assembly and therefore highlights the benefits of using $CuCrO_2$ as a novel material for DSPEC applications.

Introduction

Artificial photosynthesis offers a platform to produce a storable energy supply from fossil fuel-free resources.[1–4] This sustainable, carbon–neutral approach can produce a 'solar fuel' such as H_2 or carbon-based molecules from water or CO_2 using solar light. This process can be realised using semiconductor electrodes modified with suitable electrocatalysts in a photoelectrochemical (PEC) cell.[5–9] Electrodes featuring a molecular catalyst have advantages over 'conventional' heterogeneous systems as their 'single site catalysis' is atom-efficient,[10,11] they offer tunability and selectivity for challenging chemical transformations,[12–15] and can be rationally designed to enhance activity.[16–19] Their molecular nature also enables kinetic and mechanistic studies to reveal how they operate under various conditions, outlining routes to improvement.[20–23] Despite these advantages, the development of molecular-based photocathodes is held back by severe material limitations as state-of-the-art electrodes currently lack the requirements of visible light absorption, mesoporosity, p-type conductivity, and/or stability in aqueous solution.[5,24–27]

To bypass these limitations, a modular approach can be adopted where a visible light-absorbing dye and a molecular catalyst are co-anchored to a stable wide bandgap semiconductor platform.[7,28–30] In this dye-sensitised photoelectrochemical (DSPEC) system, the p-type semiconductor serves as the anchor site for the dye, which typically permits ultra-fast hole extraction following visible light excitation of the dye and minimises energy loss. The photoreduced dye is subsequently responsible for electron transfer to the co-immobilised electrocatalyst, where the reduction half-reaction takes place. The separation of light harvesting, charge transport, and catalysis allows the components to be individually tuned for optimal performance, where the rate of each transfer step influences the overall device efficiency.[30] A suitable pair of photoelectrodes in a tandem DSPEC cell could provide an efficient and inexpensive means of solar fuel production, exploiting simple and adaptable preparation techniques.[31–35]

The requirements for a robust DSPEC photocathode material are high p-type conductivity, propensity to anchor molecular moieties, high surface area, and a valence band position capable of readily accepting a hole from the photoexcited dye.[29,30,36] Several DSPEC photocathodes have already been reported with the majority relying on NiO,[18,37–43] and the only other examples being modified ITO[44] and $CuGaO_2$.[34] NiO is stable and easily synthesised in mesoporous form,[45–47] but suffers from the drawbacks of low charge carrier mobility and fast charge recombination between valence band holes and the reduced dye.[28,48–50] Despite many efforts and different approaches to enhance the PEC properties of dye-sensitised NiO photoelectrodes,[51–53] improvements in performance are

Christian Doppler Laboratory for Sustainable SynGas Chemistry, Department of Chemistry, Lensfield Road, Cambridge CB2 1EW, UK. E-mail: reisner@ch.cam.ac.uk
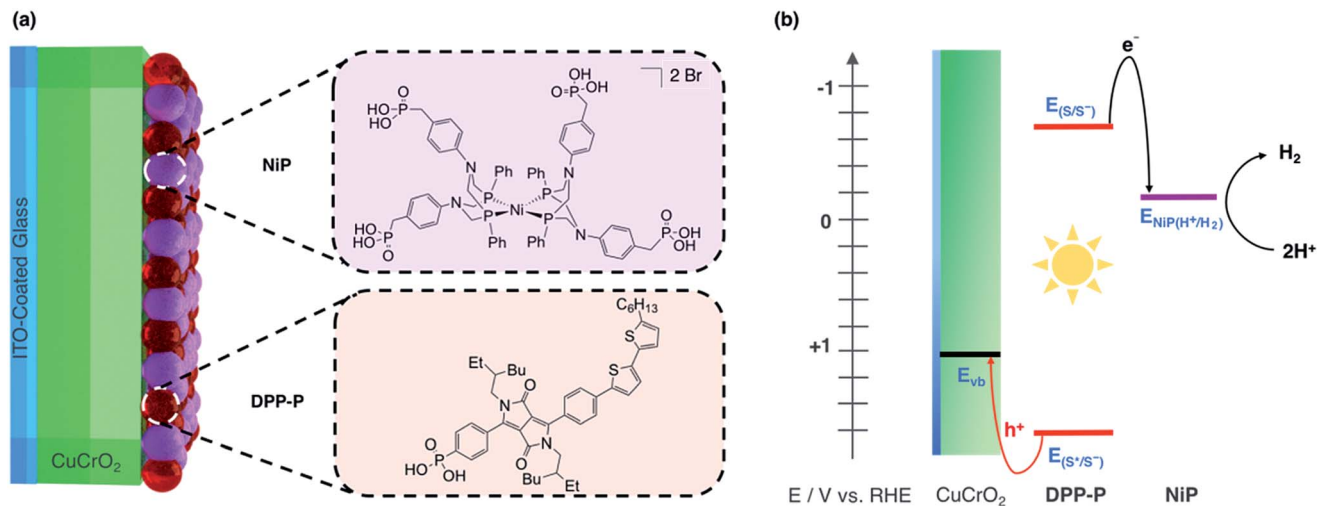
Fig. 1 (a) Dye (DPP-P) and catalyst (NiP) co-immobilised on the $CuCrO_2$ electrode with their molecular structures. (b) Energy diagram showing movement of electrons with black and holes with red arrows. S represents the dye sensitiser where $E_{(S/S^-)}$ is the ground state reduction potential and $E_{(S^*/S^-)}$ is the reduction potential in the excited state. $E_{NiP(H^+/H_2)}$ is the catalytic onset potential for NiP and E_{vb} is the $CuCrO_2$ valence band potential.

hindered by these limitations and there is a crucial need for better alternatives.

Wide bandgap Cu(I)-based mixed metal oxides such as $Cu^{I}M^{III}O_2$ delafossites (M = Co, B, In, Sc, Cr, Al, Ga) have been employed in p-type dye-sensitised solar cells (p-DSSCs),[54,55] but their incorporation in solar fuel devices is limited.[56–58] The sole example of their use with a co-immobilised dye and molecular catalyst in solar fuel generation was reported for CO_2 reduction to CO with an anchored precious metal-based **Ru–Re** dyad on a $CuGaO_2$ delafossite electrode.[34] Delafossite $CuCrO_2$ has shown promise in p-DSSCs but application has yet to be extended to DSPEC cells despite it showing clear benefits such as a low-lying valence band, high hole mobility, and simple and scalable synthesis.[59–63]

In this study, we report solar H_2 generation with dye-sensitised $CuCrO_2$ and demonstrate the feasibility of solar fuel synthesis with a $CuMO_2$ delafossite using precious metal-free dye/catalyst molecules. This was achieved by first modifying $CuCrO_2$ with a phosphonic acid-bearing diketopyrrolopyrrole-based organic dye (**DPP-P**) and characterising the PEC reduction of a soluble electron acceptor in aqueous conditions. Then, a tetraphosphonated Ni-bis(diphosphine), $[Ni(P_2N_2)_2]^{2+}$, molecular catalyst (**NiP**) was co-immobilised to determine the PEC activity for the reduction of aqueous protons (Fig. 1a). The resulting hybrid DSPEC photocathode produces H_2 at moderate applied voltages with good photocurrents. Direct comparison with a corresponding NiO photocathode highlights the benefits of $CuCrO_2$ and encourages the search for new DSPEC cathode materials.

Results and discussion

Synthesis and characterisation of $CuCrO_2$

Scalable and straightforward procedures for preparation of $CuCrO_2$ make it a highly accessible material, and its metal oxide

character ensures that molecular species can be easily attached to the surface using anchoring groups such as phosphonic acids or carboxylic acids.[59–63] In this study, $CuCrO_2$ films were grown directly on ITO-coated glass following a previously established sol–gel route.[59,60] In brief, a mixture of $Cu(acetate)_2 \cdot H_2O$ (0.2 M), $Cr(NO_3)_3 \cdot 9H_2O$ (0.2 M), and triethanolamine (0.4 M) in absolute ethanol was spin-coated on an ITO-coated glass substrate. These samples were annealed in air at 400 °C for 45 min before repeating the spin-coating and annealing steps to obtain a total of 6 layers. Post-annealing was carried out under N_2 at 600 °C for 45 min to form the delafossite structure. NiO films (2 μm thick) were prepared for comparison using a previously reported hydrothermal growth method.[37]

$CuCrO_2$ crystallises in a rhombohedral unit cell (space group $R\bar{3}m$) and is a wide bandgap p-type semiconductor (E_g = 3.1 eV) exhibiting a low-lying valence band and high hole mobility.[63,64] The structure consists of 'infinite' $[CrO_2]$ layers of edge-sharing $[CrO_6]$ octahedra linked by linear O–Cu–O dumbbells and the p-type conductivity stems predominantly from Cu^+ vacancies in the crystal lattice.[65,66] Favourable mixing of Cr 3d states with O 2p states increases the covalent nature of this interaction in the valence band, hence holes are more delocalised than in other corresponding delafossite structures, accounting for the intrinsic high hole mobility.[64,66]

X-ray diffraction (XRD) analysis confirmed the rhombohedral delafossite structure for $CuCrO_2$ (Fig. S1†) and scanning electron microscopy (SEM) images showed individual rods with a length of 73.3 ± 16.5 nm and thickness of 20.7 ± 3.7 nm, leaving a pore diameter of 16.7 ± 4.8 nm (Fig. 2a). The $CuCrO_2$ film (resulting from 6 layers) was approximately 500 nm thick. N_2 gas adsorption isotherms showed type IV behaviour consistent with a mesoporous material and gave a BET surface area of 25 m^2 g^{-1} (Fig. S2†), which is similar to that obtained with other mesoporous structures.[47] The direct bandgap of $CuCrO_2$ was estimated from a Tauc plot as 3.1 eV (Fig. S3†) and the flatband
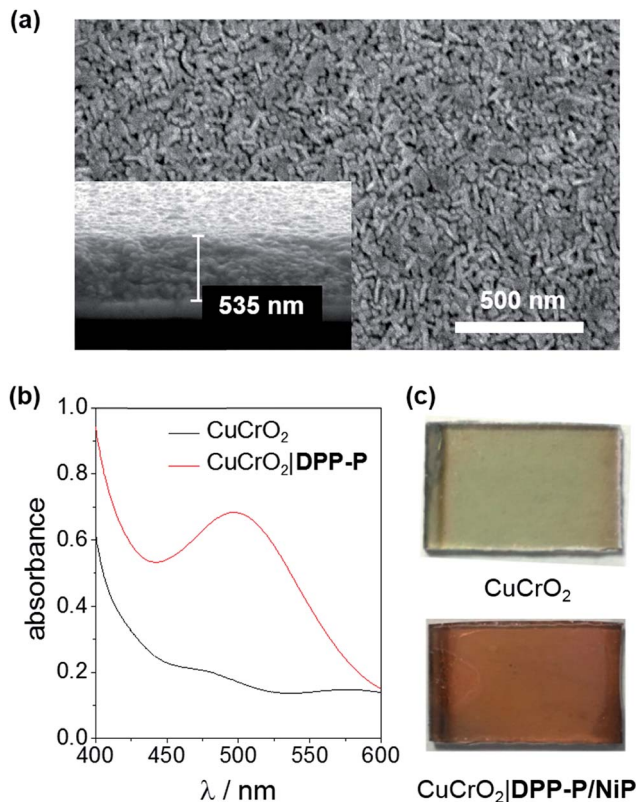
Fig. 2 (a) Top-down and cross-sectional (inset) images of a 6-layer $CuCrO_2$ electrode, (b) transmission UV-Vis spectrum of $CuCrO_2$ and $CuCrO_2$|**DPP-P** electrodes (ITO-glass background subtracted), (c) photographs of the as-prepared $CuCrO_2$ and $CuCrO_2$|**DPP-P/NiP** electrodes.

potential, E_{fb}, of +1.0 V *vs.* RHE with Mott–Schottky analysis from consecutive impedance scans (Fig. S4†). This is 0.25 V more positive than the E_{fb} of our NiO electrodes.[37] See Experimental section for more details about synthesis and characterisation of the electrodes.

Components of the molecule-loaded $CuCrO_2$ photoelectrode

As dye and catalyst species, we selected **DPP-P** and **NiP** respectively, both recently synthesised in our group (Fig. 1a).[67,68] For the most suitable light absorber, a dye with sufficient driving force to reduce the H_2 evolution catalyst as well as a thermodynamically accessible reduction potential for the extraction of holes by $CuCrO_2$ is required. Diketopyrrolopyrrole (DPP) chromophores have recently displayed high activity with NiO in p-DSSCs and are considered suitable candidates due to their high photostability, simple synthesis and modification, and lack of precious metal elements.[36] **DPP-P** absorbs strongly in the visible range ($\varepsilon_{496\ nm} = 2.6 \times 10^4$ M^{-1} cm^{-1}, DMF)[67] and is expected to undergo reductive quenching when immobilised on a p-type semiconductor due to fast hole injection originating from the proximity and good electrical communication between the dye and semiconductor.[69–74] In this pathway, the first step upon dye excitation is the reduction of **DPP-P*** by hole injection into the valence band of $CuCrO_2$, followed by oxidation of **DPP-**

P$^-$ by the catalyst, which ultimately performs the chemical reaction. **NiP**, a Dubois-type Ni-catalyst[75,76] featuring four phosphonic acid anchoring groups, has previously demonstrated reduction of aqueous protons both in solution and when immobilised on a semiconductor surface whilst maintaining molecular integrity during photocatalysis.[5,6,67,68] **DPP-P** has a reduction potential in the excited state of +1.57 V *vs.* RHE and the reduced dye has an oxidation potential of −0.7 V *vs.* RHE, thus **DPP-P**$^-$ can provide sufficient driving force for the reduction of **NiP** to a catalytically active state (onset of catalytic current for **NiP** = −0.21 V *vs.* RHE).[68] The respective electrochemical potential of each component and the hole and electron transfer pathways for the fully assembled **DPP-P/NiP**-modified $CuCrO_2$ electrode is shown in Fig. 1b and the corresponding energy diagram with possible recombination routes in Fig. S5.†

Photoelectrochemistry of $CuCrO_2$|DPP-P

To evaluate the compatibility of **DPP-P** with $CuCrO_2$ and to ensure this interface could function without the kinetic limitations imposed by immobilisation of a molecular catalyst, PEC measurements were conducted on dye-sensitised electrodes in the presence of a soluble electron acceptor. These photocathodes were prepared by soaking $CuCrO_2$ electrodes in a **DPP-P** solution (1 mM, DMF) for 15 h. The UV-Vis spectrum of the electrodes with immobilised **DPP-P** displays an absorption maximum at approximately 500 nm, consistent with the electronic transition of the free dye (Fig. 2b and c).[67] Linear sweep voltammetry (LSV) and chronoamperometry experiments were carried out in an aqueous Na_2SO_4 electrolyte solution (0.1 M, pH 3) at room temperature in a N_2-purged one-compartment three-electrode electrochemical cell using a Pt counter electrode and a Ag/AgCl/KCl$_{sat}$ reference electrode. UV-filtered simulated solar light was used for all PEC measurements (100 mW cm^{-2}, AM 1.5G, $\lambda > 420$ nm). In control experiments without the acceptor, the bare $CuCrO_2$ electrodes displayed a small cathodic dark current, which has previously been attributed to the reduction of Cu^{2+} impurities to Cu^+ with oxygen deintercalation (Fig. 3a).[77] Irradiation of the unmodified and **DPP-P** modified electrodes resulted in only minor photocurrents without a soluble acceptor ($|j| < 3$ µA cm^{-2}, 0.0 V *vs.* RHE) (Fig. 3a).

Addition of the electron acceptor 4,4′-dithiodipyridine (DTDP, 5 mM) in the electrolyte solution allows for estimation of a maximal attainable photocurrent as DTDP is known to be easily reduced in solution ($E_{red,DTDP} = -0.06$ V *vs.* RHE).[37] The electron acceptor allows the photoreduced dye to dispose of photo-electrons and to regenerate the ground state, thereby limiting the effects of reductive dye decomposition and charge recombination, and dramatically enhancing the photocathodic response for $CuCrO_2$|**DPP-P**. An absolute photocurrent response of ≈160 µA cm^{-2} (0.0 V *vs.* RHE, Fig. 3a) was observed, which indicates efficient light-induced hole injection from the dye to the valence band of $CuCrO_2$ with reduction of the acceptor by **DPP-P**$^-$. For comparison, a NiO electrode sensitised in the same manner displayed a lower maximum photocurrent ($|j| \approx 80$ µA cm^{-2}, 0.0 V *vs.* RHE), suggesting lower
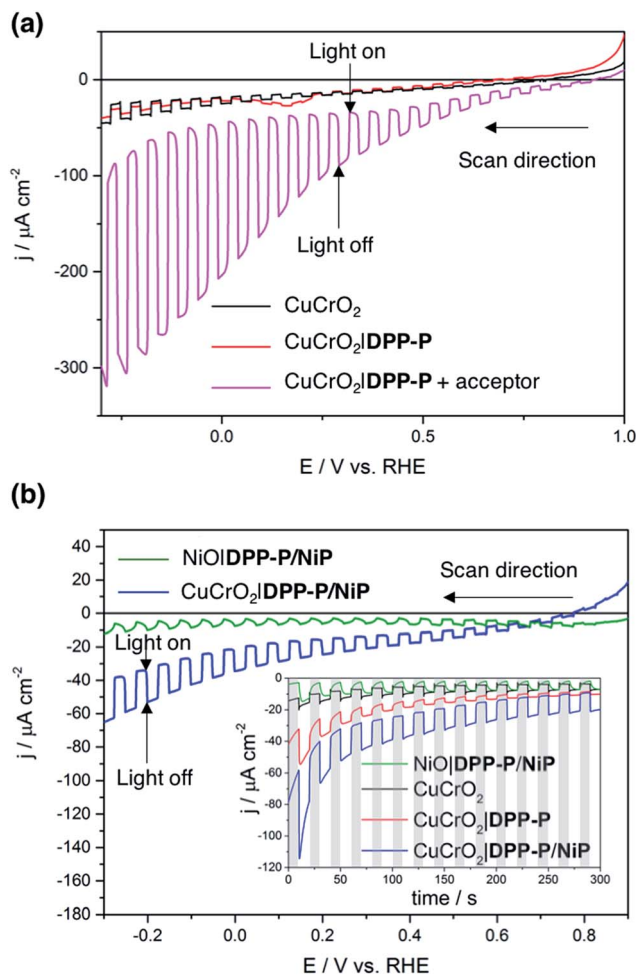
Fig. 3 Linear sweep voltammograms under chopped light illumination of (a) CuCrO$_2$ (black) and CuCrO$_2$|**DPP-P** (red) electrodes, and a CuCrO$_2$|**DPP-P** electrode with 5 mM DTDP acceptor in solution (magenta), (b) LSV scans of CuCrO$_2$|**DPP-P/NiP** (blue) and NiO|**DPP-P/NiP** (green) electrodes along with chronoamperograms (inset) of all relevant electrode compositions. The dark chops are shown with grey lines for the chronoamperograms. All experiments were performed in aqueous Na$_2$SO$_4$ electrolyte solution (0.1 M) adjusted to pH 3. Illumination with 100 mW cm^{-2}, AM 1.5G, with a 420 nm cutoff filter at room temperature. An active electrode area of 0.25 cm^2 was used with a scan rate of 5 mV s^{-1} for voltammograms.

susceptibility to recombination between the reduced dye and holes in CuCrO$_2$ (Fig. S6†). Thus, **DPP-P** displays excellent electronic communication with CuCrO$_2$, which suggests that co-anchoring of a catalyst could be a viable approach to exploit the reductive power of **DPP-P$^-$** for solar H$_2$ production.

Photoelectrochemistry with CuCrO$_2$|DPP-P/NiP

Catalyst and dye molecules were co-immobilised on CuCrO$_2$ electrodes through soaking in a solution of **NiP** (0.5 mM) and **DPP-P** (1 mM), in DMF for 15 h. The loading of **DPP-P** was quantified by UV-Vis spectroscopy following desorption in alkaline solution and the amount of immobilised **NiP** determined using inductively coupled plasma optical emission spectroscopy (ICP-OES) measurements. This resulted in a 2 : 1

ratio of dye to catalyst on the electrodes (Table S1†). Co-immobilisation of **NiP** and **DPP-P** on CuCrO$_2$ resulted in a five-fold enhancement in photocurrent compared to the bare electrode ($|j|$ = 15.1 µA cm^{-2}, 0.0 V *vs.* RHE) (Fig. 3b). This increased response is attributed to the ability of **DPP-P$^-$** to reduce **NiP** and ultimately protons.[67] This is supported by the incident photon-to-current efficiency (IPCE) spectrum, which displays a maximum photocurrent at the same wavelength as the absorption maximum of **DPP-P** (λ_{max} = 500 nm, Fig. S7†). For comparison, CuCrO$_2$ electrodes showed low efficiency and no peak at this wavelength, demonstrating the essential role of the sensitiser.

H$_2$ generation was studied using controlled potential photoelectrolysis (CPPE) under constant light illumination with an applied potential of 0.0 V *vs.* RHE. The CPPE trace of the CuCrO$_2$|**DPP-P/NiP** electrode showed high stability over a 2 hour period (Fig. S8†) with 94 ± 10 nmol of H$_2$ generated, corresponding to a turnover number of the **NiP** catalyst (TON$_{cat}$) of 126 ± 13 and a faradaic efficiency (FE) of 34 ± 8%. Possible explanations for the modest FE are the dark current originating from Cu^{2+} reduction and oxygen deintercalation,[77] as well as capacitive currents due to the mesoporous structure or from electrons trapped in surface states.[56,78–80] The FE is lowered by probable photobleaching/decomposition and desorption of the dye species, and is overall comparable to previously reported dye-sensitised photocathodes (Table 1). Control experiments without dye (CuCrO$_2$|**NiP**) or catalyst (CuCrO$_2$|**DPP-P**) produced no detectable hydrogen, confirming that the full assembly is required for catalysis. A comparable NiO|**DPP-P/NiP** electrode modified in the same manner only yielded 35 ± 2 nmol of H$_2$ after 2 hours, with a FE of 31 ± 8%, demonstrating the superior performance (2–3 times) of CuCrO$_2$ (Table 1). Accurate quantification of the Ni-catalyst loading on NiO was not possible by ICP-OES (same element in catalyst and substrate) or by UV-Vis spectroscopy following desorption (low molar absorption of **NiP**).

Post-electrolysis characterisation of CuCrO$_2$|**DPP/NiP** electrodes using ICP-OES showed that the amount of **NiP** retained on the surface after 2 h of CPPE was 54% of the initial loading (Table S1†). This is in part due to the relatively low surface area exhibited by the delafossite particulates (25 m^2 g^{-1}), which accounts for low loadings of catalyst and dye, and allows for their easy desorption into the media. Nanostructuring of the surface would ensure higher loadings of dye and catalyst species, enhancing both stability and activity in the future. Alternate methods such as atomic layer deposition (ALD)[52,81–83] or polymeric assembly[84–87] could also be employed as additional stabilisation methods.

Comparison with state-of-the-art

Limited improvements in photocathode development for DSPEC proton reduction are largely due to p-type materials with low performance. Since the first report in 1999 towards p-type DSSC, dye-sensitised NiO electrodes have generated a range of beneficial research on dye architecture and electrolyte composition.[48,88,89] Despite this, their performance remains significantly lower than their n-type counterparts, highlighting the limitations of NiO and

Table 1 Dye-sensitised photocathodes with immobilised molecular catalysts for proton reduction in aqueous solution

Substrate	Dye	Catalyst	pH	Electrolyte solution	$|j|/\mu A\ cm^{-2}$@E_{app}/V vs. RHE	Faradaic efficiency	TON_{cat}	Reference
CuCrO$_2$	**DPP-P**	**NiP**	3	Na$_2$SO$_4$	15@0.00	34 ± 8%	126 ± 13.3 (2 h)	This work
NiO	**DPP-P**	**NiP**	3	Na$_2$SO$_4$	5.8@0.00	31 ± 8%	n. r.[a]	This work
NiO	Ru complex (**RuP3**)	**NiP**	3	Na$_2$SO$_4$	~10@0.30	8.6 ± 2.3%	≈1 (2 h)[b]	37
NiO	Dyad organic dye-cobalt diimine-dioxime		5.5	MES/NaCl	15@0.14	9.5%	≈4 (2 h)[b]	18
NiO	Supramolecular Ru complex-cobaloxime assembly		7	Phosphate	8@0.51	68%	n. r.[a]	40
NiO	Organic dye (**P1**)	Cobaloxime	7	Phosphate	~5@0.21	68%	n. r.[a]	39
NiO	Ru complex (**RuP**)	Cobaloxime (**CoHEC**)	7	Phosphate	13@0.21	n. r.[a]	n. r.[a]	41
NiO	Coumarine C343	Fe$_2$(CO)$_6$(bdt)	4.5	Acetate	~10@0.16	50%	≤3 (18 min)	38
NiO	CdSe	Cobaloxime	6.8	Na$_2$SO$_4$	100@0.40	81%	n. r.[a]	42
ITO	Supramolecular Ru complex (**RuP2**)-**NiP** assembly		5.1	MES	56@0.05	53 ± 5%	≈16 (3 h)[b]	43
NiKO|NiCuO|ioITO	Supramolecular Ru complex (**RuP2**)-**NiP** assembly		5.0	MES/KCl	~59@0.05	~90%	≈20 (2 h)	44

[a] n. r.: not reported. [b] Calculated from the reference.

the need for a better alternative. Table 1 highlights relevant examples as a comparison for our system.

The TON_{cat} is a good measure of catalytic activity for a molecular catalyst-based system but remains unreported in most cases. A TON_{cat} > 125 after 2 h for our CuCrO$_2$ system in water compares favourably with the currently highest reported value of ≈20 for a NiO DSPEC photocathode.[43]

With **NiP** as the catalyst, an ITO electrode produced higher photocurrents and more H$_2$,[44] but PEC activity has only been demonstrated for an applied potential of +0.05 V vs. RHE. CuCrO$_2$ allows for a much higher working voltage due to the onset potential being situated at +0.75 V vs. RHE and therefore shows greater suitability for energy storage and implementation in tandem DSPEC cells. This photocurrent onset is also more favourable than other commonly used narrow bandgap p-type semiconductors such as GaP,[90,91] and p-Si,[5,92] highlighting the benefits of moving to dye-sensitised systems for H$_2$ generation.

CdSe-sensitised NiO produces the highest amount of H$_2$ of these electrodes over the duration of 2 hours of CPPE,[42] but a large portion of the photocurrent stems from the bare quantum dots. Despite this, sensitisation with quantum dot species is a viable approach to further enhance the H$_2$ producing capability of a CuCrO$_2$-based photocathode in the future. In comparing these properties, it is clear that material alteration can have a great influence on activity, and that transferring from NiO to CuCrO$_2$ has advantages for DSPEC applications.

Conclusions

We have introduced CuCrO$_2$ co-sensitised with an organic dye (**DPP-P**) and molecular catalyst (**NiP**) for DSPEC H$_2$ generation under aqueous conditions. CuCrO$_2$|**DPP-P**/**NiP** showed a photocurrent onset at +0.75 V vs. RHE and a photocurrent density of 15 μA cm^{-2} at 0.0 V vs. RHE with a TON_{cat} of 126 ± 13 achieved in controlled potential photoelectrolysis under UV-filtered simulated solar light irradiation. The molecule-loaded delafossite electrode therefore surpasses the performance of benchmark NiO electrodes in side-by-side comparison. We also show that the phosphonated organic DPP dye allows for high performance in aqueous conditions on an electrode and is able to electronically cooperate with **NiP**, which enabled us to assemble a fully precious metal-free DSPEC photocathode. The photocathode displays a higher photovoltage than other current state-of-the-art materials such as p-Si and GaP, making it well suited for coupling with a photoanode in tandem water splitting. Co-immobilisation of a dye and a CO$_2$ reduction catalyst on this p-type semiconductor may allow photocathodic production of carbon based fuels and chemical feedstocks.

The synthesis of CuCrO$_2$ by sol–gel techniques is straightforward and scalable. Nanostructuring would enhance the molecular loading and provide another avenue to increase photocurrents and the H$_2$ producing capability of the photocathode. Material alteration, for example through Mg^{2+} doping,[62] could also improve the activity by further enhancing conductivity and therefore charge extraction through the film. Other methods to improve the separation between catalyst and the delafossite surface would also

enhance the efficiency by reducing charge recombination.[37] This work demonstrates the benefit of adopting new delafossite structures as p-type semiconductors for solar fuel generation.

Experimental section

Materials and methods

NiP[68] and **DPP-P**[67] were synthesised according to previously reported methods. Cu(acetate)$_2$·H$_2$O (ACROS Organics, ACS reagent), Cr(NO$_3$)$_3$·9H$_2$O (Sigma-Aldrich, ≥99%), and triethanolamine (Sigma-Aldrich, ≥99.5%) were used to prepare CuCrO$_2$. ITO-coated glass substrates (Vision Tek Systems Ltd., R = 12 Ω cm^{-2}, thickness = 1.1 mm) were cut into 3 × 3 cm^2 squares and scored into 1 × 1.5 cm^2 divisions before cleaning. Milli-Q® H$_2$O (R > 18.2 MΩ cm) was used for all electrochemical and analytical measurements. DTDP (Sigma-Aldrich, 98%) was used as an electron acceptor at a concentration of 5 mM. Addition of DTDP resulted in a change in pH of the electrolyte solution from 3 to 4.6.

Preparation of CuCrO$_2$ electrodes

ITO-coated glass was cleaned through successive sonication in isopropanol, ethanol, and acetone for 15 min each, followed by drying at 100 °C in air before use. A mixture of Cu(acetate)$_2$·H$_2$O (0.2 M), and triethanolamine (0.4 M) in absolute ethanol was stirred for 1 h before addition of Cr(NO$_3$)$_3$·9H$_2$O (0.2 M). This solution was kept stirring for 15 h before being spin-coated on the ITO-glass slides (Laurell WS-650MZ spin coater, 1500 rpm, 15 s, 3000 rpm s^{-1} acceleration, 0.4 mL volume). The slides were annealed in air to 400 °C for 45 min with a ramp rate of 10 °C min^{-1} in a chamber furnace (Carbolite Gero). These steps were repeated to form 6 layers. The final annealing step involved heating in a N$_2$ atmosphere to 600 °C for 45 min with a ramp rate of 5 °C min^{-1} using a tube furnace fitted with a quartz tube, end seals, and insulation plugs (Carbolite Gero). The electrodes were left to cool to room temperature and used as-prepared without any additional treatment.

Material characterisation

XRD measurements were conducted using a PANalytical BV X'Pert Pro X-ray diffractometer. SEM images were taken using a FEI Phillips XL30 sFEG microscope. UV-Vis absorption spectra were obtained using a Varian Cary 50 spectrophotometer in transmission mode.

N$_2$ gas adsorption measurements

Adsorption isotherms were carried out using a Micromeritics 3 Flex (Micromiretics, Norcross, GA, USA) with N$_2$ as the adsorbate. Samples were prepared on glass slides then scraped from the surface. Degassing for 10 h at 110 °C was required prior to measurements, which were carried out in liquid N$_2$. The BET specific surface area was obtained by fitting N$_2$ isotherms using the Microactive software.

Mott–Schottky analysis

Electrochemical impedance spectroscopy (EIS) measurements were conducted using an IviumStat potentiostat at 25 °C using a 3-necked round-bottomed flask under dark conditions. A three-electrode setup using a Pt mesh counter, Ag/AgCl/KCl$_{sat}$ reference, and a CuCrO$_2$ working electrode (0.25 cm^2 active area) was used with an electrolyte solution of Na$_2$SO$_4$ (0.1 M, pH 3). The frequency range was 10 kHz to 0.01 Hz, with an excitation voltage of 10 mV. Nyquist plots obtained in the potential range 1.1 V to 0.3 V vs. RHE (15 mV step) were fitted using ZView® (Scribner Associates Inc.) to a Randles circuit (inset Fig. S4†) to obtain interfacial capacitance (C_{sc}) values. The Mott–Schottky equation, $\frac{1}{C_{sc}^2} = \frac{2}{\varepsilon\varepsilon_0 A^2 eN}\left(E - E_{fb} - \frac{k_B T}{e}\right)$, was used to obtain an estimate of the flatband potential through a plot of $1/C_{sc}^2$ against the applied potential. A negative slope indicated p-type character and the x-intercept is equal to E_{fb} + $k_B T/e$.[37]

Electrochemical measurements

Cyclic voltammetry was used to determine the reduction potential of the **DPP-P** dye, $E_{(S/S^-)}$, from the half-wave potential. This was performed in a 3-electrode setup with a glassy carbon working electrode, Pt-mesh counter electrode, and a Ag/AgCl/KCl$_{sat}$ reference electrode with a scan rate of 50 mV s^{-1}. The electrolyte solution consisted of tetrabutylammonium tetrafluoroborate (0.1 M) in dry DMF with the addition of **DPP-P** (around 0.1 M). Addition of the E_{00} to $E_{(S/S^-)}$ provides an estimate for the excited state reduction potential, $E_{(S^*/S^-)}$.

Modification of electrodes with dye and catalyst species

Molecular species were co-immobilised through soaking in a bath consisting of **DPP-P** (1 mM) and **NiP** (0.5 mM) in DMF for 15 h. For CuCrO$_2$|**DPP-P** and CuCrO$_2$|**NiP** electrodes the concentration was 1 mM but all other conditions kept the same. All electrodes were rinsed with DMF and H$_2$O then dried in air and stored in the dark before use.

Quantification of loaded DPP-P and NiP

DPP-P was desorbed from CuCrO$_2$|**DPP-P/NiP** electrodes using a solution of 0.1 M tetrabutylammonium hydroxide 30-hydrate in DMF (1 mL) and the absorption at 500 nm was determined using UV-Vis spectroscopy. A calibration curve was used to fit values and determine the loading for 4 different electrodes. **NiP** was quantified by ICP-OES after digestion of CuCrO$_2$|**DPP-P/NiP** electrodes (1 cm^2 film area) in aqueous HNO$_3$ (70%, 1 mL) overnight and dilution to 10% v/v with MilliQ® water. CuCrO$_2$|**DPP-P/NiP** electrodes pre- and post-electrolysis were analysed along with blanks for nitric acid, CuCrO$_2$, and CuCrO$_2$|**DPP-P** in triplicate. Errors represent standard deviation from the mean.[37]

PEC measurements

Photoelectrochemical measurements were carried out using an Ivium CompactStat potentiostat in a one-compartment three-

necked custom made cell equipped with a flat borosilicate glass window. A three-electrode setup was used with a Pt-counter electrode, a Ag/AgCl/KCl$_{sat}$ reference, and the working electrode consisted of the CuCrO$_2$ platform with an illuminated area of 0.25 cm^2 confined using electrical tape. All measurements were conducted using aqueous Na$_2$SO$_4$ electrolyte solution (0.1 M, pH 3) and the cell was purged with N$_2$ for 15 min prior to experiments. Frontside illumination was used for all experiments using a calibrated Newport Oriel solar light simulator (150 W, 100 mW cm^{-2}, AM 1.5G) fitted with a UQG Optics UV Filter ($\lambda > 420$ nm) and IR water filter.

CPPE experiments were carried out in a custom two-compartment airtight electrochemical cell separated by a Nafion membrane and featuring a flat quartz glass window. The volume of electrolyte solution in the working compartment was 12 mL with a gas headspace of 5 mL while the counter compartment consisted of 4.5 mL solution and a 3.5 mL headspace. Prior to electrolysis, the gas headspace was purged for 30 min with 2% CH$_4$ in N$_2$. An Agilent 7890A series gas chromatograph with a 5 Å molecular sieve column and a thermal conductivity detector was used to quantify the amount of H$_2$ produced. The oven temperature was kept constant at 45 °C and the flow rate was 3 mL min^{-1}. The partial pressure of H$_2$ was calculated to account for dissolved H$_2$ and this was added to the overall amount of hydrogen generated to obtain the faradaic efficiency. All CPPE experiments were carried out in triplicate with an applied potential of 0.0 V *vs.* RHE.

IPCE measurements

IPCE spectra were recorded in a N$_2$-purged three-necked one-compartment custom cell with a flat borosilicate glass window. A three-electrode setup with Pt counter, Ag/AgCl/KCl$_{sat}$ reference, and working electrode was used with pH 3 Na$_2$SO$_4$ electrolyte solution (0.1 M). Monochromatic light was provided using a 300 W Xenon lamp solar light simulator coupled to a monochromator (MSH300, LOT Quantum design) and the intensity calibrated to 0.8 mW cm^{-2} for each wavelength. The potential was maintained at 0.0 V *vs.* RHE for all wavelengths and photocurrents were recorded in triplicate with different electrodes (0.25 cm^2 active area) for both CuCrO$_2$ and CuCrO$_2$-|**DPP-P/NiP** arrangements.

Conflicts of interest

There are no conflicts to declare.

Acknowledgements

References

1 Y. Tachibana, L. Vayssieres and J. R. Durrant, *Nat. Photonics*, 2012, **6**, 511–518.

2 J. Willkomm, K. L. Orchard, A. Reynal, E. Pastor, J. R. Durrant and E. Reisner, *Chem. Soc. Rev.*, 2015, **45**, 9–23.

3 M. G. Walter, E. L. Warren, J. R. McKone, S. W. Boettcher, Q. Mi, E. A. Santori and N. S. Lewis, *Chem. Rev.*, 2010, **110**, 6446–6473.

4 D. Gust, T. A. Moore and A. L. Moore, *Acc. Chem. Res.*, 2009, **42**, 1890–1898.

5 J. J. Leung, J. Warnan, D. H. Nam, J. Z. Zhang, J. Willkomm and E. Reisner, *Chem. Sci.*, 2017, **8**, 5172–5180.

6 T. E. Rosser, M. A. Gross, Y.-H. Lai and E. Reisner, *Chem. Sci.*, 2016, **7**, 4024–4035.

7 M. K. Brennaman, R. J. Dillon, L. Alibabaei, M. K. Gish, C. J. Dares, D. L. Ashford, R. L. House, G. J. Meyer, J. M. Papanikolas and T. J. Meyer, *J. Am. Chem. Soc.*, 2016, **138**, 13085–13102.

8 N. Queyriaux, N. Kaeffer, A. Morozan, M. Chavarot-Kerlidou and V. Artero, *J. Photochem. Photobiol., C*, 2015, **25**, 90–105.

9 K. Sivula and R. van de Krol, *Nat. Rev. Mater.*, 2016, **1**, 15010.

10 M. P. Stewart, M. H. Ho, S. Wiese, M. Lou Lindstrom, C. E. Thogerson, S. Raugei, R. M. Bullock and M. L. Helm, *J. Am. Chem. Soc.*, 2013, **135**, 6033–6046.

11 G. Sahara and O. Ishitani, *Inorg. Chem.*, 2015, **54**, 5096–5104.

12 D.-I. Won, J. S. Lee, J. M. Ji, W. J. Jung, H. J. Son, C. Pac and S. O. Kang, *J. Am. Chem. Soc.*, 2015, **137**, 13679–13690.

13 M. F. Kuehnel, K. L. Orchard, K. E. Dalle and E. Reisner, *J. Am. Chem. Soc.*, 2017, **139**, 7217–7223.

14 S. Roy, B. Sharma, J. Pécaut, P. Simon, M. Fontecave, P. D. Tran, E. Derat and V. Artero, *J. Am. Chem. Soc.*, 2017, **139**, 3685–3696.

15 B. Reuillard, K. H. Ly, T. E. Rosser, M. F. Kuehnel, I. Zebger and E. Reisner, *J. Am. Chem. Soc.*, 2017, **139**, 14425–14435.

16 J. Willkomm, N. M. Muresan and E. Reisner, *Chem. Sci.*, 2015, **6**, 2727–2736.

17 K. Sekizawa, K. Maeda, K. Domen, K. Koike and O. Ishitani, *J. Am. Chem. Soc.*, 2013, **135**, 4596–4599.

18 N. Kaeffer, J. Massin, C. Lebrun, O. Renault, M. Chavarot-Kerlidou and V. Artero, *J. Am. Chem. Soc.*, 2016, **138**, 12308–12311.

19 Y. Tamaki and O. Ishitani, *ACS Catal.*, 2017, **7**, 3394–3409.

20 A. Reynal, F. Lakadamyali, M. A. Gross, E. Reisner and J. R. Durrant, *Energy Environ. Sci.*, 2013, **6**, 3291–3300.

21 G. Neri, M. Forster, J. J. Walsh, C. M. Robertson, T. J. Whittles, P. Farràs and A. J. Cowan, *Chem. Commun.*, 2016, **52**, 14200–14203.

22 E. Pastor, F. Le Formal, M. T. Mayer, S. D. Tilley, L. Francàs, C. A. Mesa, M. Grätzel and J. R. Durrant, *Nat. Commun.*, 2017, **8**, 14280.

23 T. E. Rosser and E. Reisner, *ACS Catal.*, 2017, **7**, 3131–3141.

24 M. Schreier, J. Luo, P. Gao, T. Moehl, M. T. Mayer and M. Grätzel, *J. Am. Chem. Soc.*, 2016, **138**, 1938–1946.

25 L. Ji, M. D. McDaniel, S. Wang, A. B. Posadas, X. Li, H. Huang, J. C. Lee, A. A. Demkov, A. J. Bard, J. G. Ekerdt and E. T. Yu, *Nat. Nanotechnol.*, 2014, **10**, 84–90.

26 S. Hu, N. S. Lewis, J. W. Ager, J. Yang, J. R. McKone and N. C. Strandwitz, *J. Phys. Chem. C*, 2015, **119**, 24201–24228.

27 M. Crespo-Quesada and E. Reisner, *Energy Environ. Sci.*, 2017, **10**, 1116–1127.

28 P. Xu, N. S. McCool and T. E. Mallouk, *Nano Today*, 2017, **14**, 42–58.

29 Z. Yu, F. Li and L. Sun, *Energy Environ. Sci.*, 2015, **8**, 760–775.

30 E. A. Gibson, *Chem. Soc. Rev.*, 2017, **46**, 6194–6209.

31 M. S. Prévot and K. Sivula, *J. Phys. Chem. C*, 2013, **117**, 17879–17893.

32 G. Sahara, H. Kumagai, K. Maeda, N. Kaeffer, V. Artero, M. Higashi, R. Abe and O. Ishitani, *J. Am. Chem. Soc.*, 2016, **138**, 14152–14158.

33 F. F. Abdi, L. Han, A. H. M. Smets, M. Zeman, B. Dam and R. van de Krol, *Nat. Commun.*, 2013, **4**, 2195.

34 H. Kumagai, G. Sahara, K. Maeda, M. Higashi, R. Abe and O. Ishitani, *Chem. Sci.*, 2017, **8**, 4242–4249.

35 K. Fan, F. S. Li, L. Wang, Q. Daniel, E. Gabrielsson and L. C. Sun, *Phys. Chem. Chem. Phys.*, 2014, **16**, 25234–25240.

36 Y. Farré, L. Zhang, Y. Pellegrin, A. Planchat, E. Blart, M. Boujtita, L. Hammarström, D. Jacquemin and F. Odobel, *J. Phys. Chem. C*, 2016, **120**, 7923–7940.

37 M. A. Gross, C. E. Creissen, K. L. Orchard and E. Reisner, *Chem. Sci.*, 2016, **7**, 5537–5546.

38 L. J. Antila, P. Ghamgosar, S. Maji, H. Tian, S. Ott and L. Hammarström, *ACS Energy Lett.*, 2016, **1**, 1106–1111.

39 F. Li, K. Fan, B. Xu, E. Gabrielsson, Q. Daniel, L. Li and L. Sun, *J. Am. Chem. Soc.*, 2015, **137**, 9153–9159.

40 Z. Ji, M. He, Z. Huang, U. Ozkan and Y. Wu, *J. Am. Chem. Soc.*, 2013, **135**, 11696–11699.

41 K. Fan, F. Li, L. Wang, Q. Daniel, E. Gabrielsson and L. Sun, *Phys. Chem. Chem. Phys.*, 2014, **16**, 25234–25240.

42 P. Meng, M. Wang, Y. Yang, S. Zhang and L. Sun, *J. Mater. Chem. A*, 2015, **3**, 18852–18859.

43 B. Shan, B. D. Sherman, C. M. Klug, A. Nayak, S. L. Marquard, Q. Liu, R. M. Bullock and T. J. Meyer, *J. Phys. Chem. Lett.*, 2017, **8**, 4374–4379.

44 B. Shan, A. Das, S. L. Marquard, B. H. Farnum, D. Wang, R. M. M. Bullock and T. J. Meyer, *Energy Environ. Sci.*, 2016, **9**, 3693–3697.

45 L. Lepleux, B. Chavillon, Y. Pellegrini, E. Blart, L. Cario, S. Jobic and F. Odobel, *Inorg. Chem.*, 2009, **48**, 8245–8250.

46 E. A. Gibson, M. Awais, D. Dini, D. P. Dowling, M. T. Pryce, J. G. Vos and A. Hagfeldt, *Phys. Chem. Chem. Phys.*, 2013, **15**, 2411–2420.

47 C. J. Wood, G. H. Summers, C. A. Clark, N. Kaeffer, M. Braeutigam, L. R. Carbone, L. D'Amario, K. Fan, Y. Farré, S. Narbey, F. Oswald, L. A. Stevens, C. D. J. Parmenter, M. W. Fay, A. La Torre, C. E. Snape, B. Dietzek, D. Dini, L. Hammarström, Y. Pellegrin, F. Odobel, L. Sun, V. Artero and E. A. Gibson, *Phys. Chem. Chem. Phys.*, 2016, **18**, 10727–10738.

48 F. Odobel, Y. Pellegrin, E. A. Gibson, A. Hagfeldt, A. L. Smeigh and L. Hammarström, *Coord. Chem. Rev.*, 2012, **256**, 2414–2423.

49 A. Morandeira, J. Fortage, T. Edvinsson, L. Le Pleux, E. Blart, G. Boschloo, A. Hagfeldt, L. Hammarström and F. Odobel, *J. Phys. Chem. C*, 2008, **112**, 1721–1728.

50 Z. Huang, G. Natu, Z. Ji, M. He, M. Yu and Y. Wu, *J. Phys. Chem. C*, 2012, **116**, 26239–26246.

51 K. A. Click, D. R. Beauchamp, Z. Huang, W. Chen and Y. Wu, *J. Am. Chem. Soc.*, 2016, **138**, 1174–1179.

52 R. J. Kamire, M. B. Majewski, W. L. Hoffeditz, B. T. Phelan, O. K. Farha, J. T. Hupp and M. R. Wasielewski, *Chem. Sci.*, 2017, **8**, 541–549.

53 C. J. Flynn, S. M. McCullough, E. Oh, L. Li, C. C. Mercado, B. H. Farnum, W. Li, C. L. Donley, W. You, A. J. Nozik, J. R. McBride, T. J. Meyer, Y. Kanai and J. F. Cahoon, *ACS Appl. Mater. Interfaces*, 2016, **8**, 4754–4761.

54 I. Sullivan, B. Zoellner and P. A. Maggard, *Chem. Mater.*, 2016, **28**, 5999–6016.

55 M. Yu, T. I. Draskovic and Y. Wu, *Phys. Chem. Chem. Phys.*, 2014, **16**, 5026–5033.

56 M. S. Prévot, X. A. Jeanbourquin, W. S. Bourée, F. Abdi, D. Friedrich, R. van de Krol, N. Guijarro, F. Le Formal and K. Sivula, *Chem. Mater.*, 2017, **29**, 4952–4962.

57 M. S. Prévot, N. Guijarro and K. Sivula, *ChemSusChem*, 2015, **8**, 1359–1367.

58 J. Gu, Y. Yan, J. W. Krizan, Q. D. Gibson, Z. M. Detweiler, R. J. Cava and A. B. Bocarsly, *J. Am. Chem. Soc.*, 2014, **136**, 830–833.

59 A. K. Díaz-García, T. Lana-Villarreal and R. Gómez, *J. Mater. Chem. A*, 2015, **3**, 19683–19687.

60 S. Götzendörfer, C. Polenzky, S. Ulrich and P. Löbmann, *Thin Solid Films*, 2009, **518**, 1153–1156.

61 S. Powar, D. Xiong, T. Daeneke, M. T. Ma, A. Gupta, G. Lee, S. Makuta, Y. Tachibana, W. Chen, L. Spiccia, Y. B. Cheng, G. Götz, P. Bäuerle and U. Bach, *J. Phys. Chem. C*, 2014, **118**, 16375–16379.

62 D. Xiong, W. Zhang, X. Zeng, Z. Xu, W. Chen, J. Cui, M. Wang, L. Sun and Y. B. Cheng, *ChemSusChem*, 2013, **6**, 1432–1437.

63 D. Xiong, Z. Xu, X. Zeng, W. Zhang, W. Chen, X. Xu, M. Wang and Y. B. Cheng, *J. Mater. Chem.*, 2012, **22**, 24760–24768.

64 D. O. Scanlon, K. G. Godinho, B. J. Morgan and G. W. Watson, *J. Chem. Phys.*, 2010, **132**, 24707.

65 T. Jiang, X. Li, M. Bujoli-Doeuff, E. Gautron, L. Cario, S. Jobic and R. Gautier, *Inorg. Chem.*, 2016, **55**, 7729–7733.

66 D. O. Scanlon and G. W. Watson, *J. Mater. Chem.*, 2011, **21**, 3655–3663.

67 J. Warnan, J. Willkomm, J. N. Ng, R. Godin, S. Prantl, J. R. Durrant and E. Reisner, *Chem. Sci.*, 2017, **8**, 3070–3079.

68 M. A. Gross, A. Reynal, J. R. Durrant and E. Reisner, *J. Am. Chem. Soc.*, 2014, **136**, 356–366.

69 A. M. Brown, L. J. Antila, M. Mirmohades, S. Pullen, S. Ott and L. Hammarström, *J. Am. Chem. Soc.*, 2016, **138**, 8060–8063.

70 F. A. Black, C. A. Clark, G. H. Summers, I. P. Clark, M. Towrie, T. Penfold, M. W. George and E. A. Gibson, *Phys. Chem. Chem. Phys.*, 2017, **19**, 7877–7885.

71 B. Dhital, V. G. Rao and H. P. Lu, *Phys. Chem. Chem. Phys.*, 2017, **19**, 17216–17223.

72 A. L. Smeigh, L. Le Pleux, J. Fortage, Y. Pellegrin, E. Blart, F. Odobel and L. Hammarström, *Chem. Commun.*, 2012, **48**, 678–680.

73 M. Borgström, E. Blart, G. Boschloo, E. Mukhtar, A. Hagfeldt, L. Hammarström and F. Odobel, *J. Phys. Chem. B*, 2005, **109**, 22928–22934.

74 L. Zhang, L. Favereau, Y. Farré, E. Mijangos, Y. Pellegrin, E. Blart, F. Odobel and L. Hammarström, *Phys. Chem. Chem. Phys.*, 2016, **18**, 18515–18527.

75 M. L. Helm, M. P. Stewart, R. M. Bullock, M. R. DuBois and D. L. DuBois, *Science*, 2011, **333**, 863–866.

76 W. J. Shaw, M. L. Helm and D. L. Du Bois, *Biochim. Biophys. Acta, Bioenerg.*, 2013, **1827**, 1123–1139.

77 W. Ketir, A. Bouguelia and M. Trari, *Desalination*, 2009, **244**, 144–152.

78 J. Bisquert, *Phys. Chem. Chem. Phys.*, 2003, **5**, 5360–5364.

79 L. Bertoluzzi, P. Lopez-Varo, J. A. Jiménez Tejada and J. Bisquert, *J. Mater. Chem. A*, 2016, **4**, 2873–2879.

80 J. Bisquert, *Phys. Chem. Chem. Phys.*, 2008, **10**, 49–72.

81 A. M. Lapides, B. D. Sherman, M. K. Brennaman, C. J. Dares, K. R. Skinner, J. L. Templeton and T. J. Meyer, *Chem. Sci.*, 2015, **6**, 6398–6406.

82 H. J. Son, C. Prasittichai, J. E. Mondloch, L. Luo, J. Wu, D. W. Kim, O. K. Farha and J. T. Hupp, *J. Am. Chem. Soc.*, 2013, **135**, 11529–11532.

83 D. Wang, M. V. Sheridan, B. Shan, B. H. Farnum, S. L. Marquard, B. D. Sherman, M. S. Eberhart, A. Nayak, C. J. Dares, A. K. Das, R. M. Bullock and T. J. Meyer, *J. Am. Chem. Soc.*, 2017, **139**, 14518–14525.

84 B. Reuillard, J. Warnan, J. J. Leung, D. W. Wakerley and E. Reisner, *Angew. Chem., Int. Ed.*, 2016, **55**, 3952–3957.

85 S. K. Ibrahim, X. Liu, C. Tard and C. J. Pickett, *Chem. Commun.*, 2007, 1535–1537.

86 D. H. Pool and D. L. DuBois, *J. Organomet. Chem.*, 2009, **694**, 2858–2865.

87 A. Krawicz, J. Yang, E. Anzenberg, J. Yano, I. D. Sharp and G. F. Moore, *J. Am. Chem. Soc.*, 2013, **135**, 11861–11868.

88 F. Odobel and Y. Pellegrin, *J. Phys. Chem. Lett.*, 2013, **4**, 2551–2564.

89 J. He, H. Lindström, A. Hagfeldt and S.-E. Lindquist, *J. Phys. Chem. B*, 1999, **103**, 8940–8943.

90 A. M. Beiler, D. Khusnutdinova, S. I. Jacob and G. F. Moore, *ACS Appl. Mater. Interfaces*, 2016, **8**, 10038–10047.

91 D. Khusnutdinova, A. M. Beiler, B. L. Wadsworth, S. I. Jacob and G. F. Moore, *Chem. Sci.*, 2017, **8**, 253–259.

92 C. A. Downes and S. C. Marinescu, *J. Am. Chem. Soc.*, 2015, **137**, 13740–13743.